Recent Progress in SOFC Anodes for Direct Utilization of Hydrocarbons

M. D. Gross, J. M. Vohs, and R. J. Gorte

Department of Chemical & Biomolecular Engineering,

University of Pennsylvania,

Philadelphia, PA 19104 USA

Abstract

There would be significant advantages to having anodes for solid oxide fuel cells (SOFC) that were capable of directly utilizing hydrocarbon fuels. Because conventional Ni-based anodes catalyze the formation of carbon fibers, new anode compositions are required for this application, but most of the materials that have been proposed exhibit either limited thermal stability or poor electrochemical activity. In this paper, we will describe two strategies for the development of new anodes with improved performance. The first strategy involves the use of bimetallic compositions with layered microstructures. In the bimetallic anodes, one metal is used for thermal stability while the other provides the required carbon tolerance. The second strategy involves separating the anode into two layers: a thin functional layer for electrocatalysis and a thicker conduction layer for current collection. With this approach, the functional layer can be optimized for catalytic activity and, if it is thin enough, requires minimal conductivity. Examples are shown for each of these approaches and possible future directions are outlined.

***Corresponding author**: gorte@seas.upenn.edu; FAX: 215/573-2093.

Key Words: solid-oxide fuel cell, direct oxidation, hydrocarbons, Cu, yttria-stabilized zirconia, ceria, $SrTiO_3$

Introduction

Solid oxide fuel cells (SOFC) have received a great deal of attention in recent years because they offer the promise of very high efficiency with relatively low sensitivity to impurities in the fuel [1]. Both of these properties result from the high operating temperatures, which, depending on the system design and the materials used, range from roughly 873 to 1273 K. In this temperature range, the electrode reactions are relatively fast, so that high cathode over-potentials found with low-temperature proton-exchange-membrane (PEM) fuel cells can be much lower [2]. Furthermore, the waste heat in an SOFC is produced at a temperature the heat can be used [3]. Regarding impurities, CO, a severe poison for low-temperature fuel cells, is a fuel for SOFC. While SOFC are sensitive to sulfur, they are much less sensitive than PEM fuel cells. There is even a recent claim of a high-performance SOFC that can tolerate 50 ppm H_2S when operating on H_2 [4].

The operating principles behind SOFC involve reduction of molecular O_2 at the cathode, diffusion of the oxygen anions through a ceramic electrolyte (usually yttria-stabilized zirconia, YSZ), and oxidation of the fuel by the oxygen anions at the anode. The primary reasons for requiring high operating temperatures are to achieve sufficient oxygen-anion mobility in the electrolyte and to decrease impedance losses in the electrodes. When operating YSZ-based cells on humidified H_2, the open-circuit voltage (OCV) is usually very close to the Nernst Potential, the thermodynamic limit; but cell potentials drop as current is drawn. In many cases, the cell potential drops linearly with the current density, so that the losses in the cell can be described by a sum of the individual impedances for the cathode, electrolyte, and anode. While it is difficult to separate the impedances of the two electrodes, the resistance of the electrolyte can be easily separated from the electrode losses by impedance spectroscopy [5].

When using hydrocarbons as the source of energy, it is usually assumed that SOFC must operate on syngas, a mixture of CO and H_2 produced by reforming; however, the relatively high operating temperatures of SOFC make it feasible to feed hydrocarbons directly to the anode without external reforming [6]. Direct utilization of hydrocarbons could simplify the use of fuel cells operating on hydrocarbons and significantly improve efficiency by avoiding the losses associated with external reformers [7]. The primary factor preventing direct hydrocarbon utilization in state-of-the-art fuel cells is that the Ni-based anodes are unstable in the presence of hydrocarbons unless large amounts of steam are also present.

Ni-based anodes are unstable in hydrocarbons because Ni is a catalyst for the formation of carbon fibers [7-9]. The mechanism for carbon fiber formation on Ni involves deposition of carbon on the Ni surface, dissolution of the carbon into the bulk of the Ni, and the precipitation of carbon as a fiber [9]. Because these reactions involve more than the Ni surface, carbon-fiber formation can lead to loss of Ni by "metal dusting" [10], a process that occurs when Ni is physically lifted from the sample by its attachment to the growing carbon fiber. Fiber growth can also cause fuel cells to fracture because of the mechanical stresses induced by the growth of the fibers [11].

Carbon fiber formation on Ni can be avoided if there is sufficient steam so as to remove carbon faster than it deposits. While it is often assumed that thermodynamics can be used to predict the H_2O:C ratios required to avoid carbon [12], fibers can and do form at H_2O:C ratios that are much higher than would be predicted from equilibrium calculations [8], demonstrating that it is the relative rates of carbon deposition and carbon removal that determine stability of Ni anodes. Because the rate of carbon deposition with CH_4 is relatively low, the required H_2O:C ratio for avoiding carbon is approximately one, making direct utilization of CH_4 with added

steam (i.e. internal reforming) feasible. Because carbon deposition rates on Ni are much higher with hydrocarbons larger than methane [13], higher H_2O:C ratios are required for preventing carbon fibers. While stable operation with higher hydrocarbons has been demonstrated on Ni-based anodes in the laboratory under special conditions, the intrinsic instability of the system and the catastrophic consequences of fiber formation (i.e. cell fracture and loss of Ni) make application of this approach impractical.

An alternative approach for direct utilization in SOFC is to prepare anodes from materials that do not catalyze the formation of carbon fibers the way Ni does. For example, conductive ceramics and metals like Cu, Ag, and Au do not form carbon fibers because they do not dissolve large amounts of carbon in the way that Ni, Fe, Co and Ru do [9,14]. Carbon deposits can still form at the surface of any material due to condensation of polyaromatic species formed by gas-phase pyrolysis [8]; but these deposits are not destructive in the way that fiber formation is because the carbon remains at the electrode surface. Furthermore, avoiding these deposits is relatively easy through catalytic coatings, such as ceria, which will catalyze the oxidation of these deposits in the presence of moderate amounts of steam [8]. The problem with most alternative anode materials is that their performance has not usually matched that of the best Ni anodes. For example, with Cu-based anodes, the key issue is the relatively poor thermal stability caused by metal sintering [15,16]. The main problems confronting ceramic anodes are low conductivity and poor catalytic activity [17].

In this paper, we will discuss strategies that have been used to develop alternative anodes for the direct utilization of hydrocarbons. This is a progress report and it will be obvious that there is still much work to do.

Electrode Fabrication by Impregnation

The most commonly used SOFC electrode materials are Ni-YSZ composites for the anode and Sr-doped $LaMnO_3$ (LSM)-YSZ composites for the cathode [18]. The YSZ in the composite electrodes plays a number of important roles, the most important being that it provides a good ion-conducting interface with the YSZ electrolyte, transporting oxygen ions into the electrodes and increasing the length of the three-phase boundary (TPB). Because the reactivity of YSZ with both NiO and LSM is relatively low, Ni-YSZ and LSM-YSZ electrodes can be fabricated by simply mixing YSZ powder with either NiO or LSM, followed by high-temperature sintering. NiO-YSZ composites are easily reduced to form Ni-YSZ electrodes with good conductivity and porosity.

However, the development of new electrode compositions has required new fabrication methods. For example, Cu-YSZ, ceramic-metallic (cermet) composites cannot be prepared by co-firing of CuO and YSZ due to the low melting temperature of CuO and the tendency of CuO to react with YSZ at YSZ sintering temperatures. The method developed to produce Cu-YSZ composites involved synthesizing a porous YSZ layer on the dense YSZ electrolyte, with Cu being added to the sintered porous YSZ by infiltration with soluble salts and subsequent reduction of those salts [19-21]. By sintering the porous YSZ together with the dense YSZ electrolyte, prior to the addition of Cu, the treatment temperatures for the metal and YSZ components of the cermet can be different, thus avoiding the problems associated with CuO melting and solid-state reactions. A schematic of composite fabrication by impregnation is shown in Fig. 1.

The impregnation method for electrode fabrication has been shown to be very flexible, allowing the synthesis of anode and cathode composites with a wide range of compositions

[12,22-26]. In addition to avoiding solid-state reactions, composites formed by impregnation have the additional advantage of forming a non-random structure. Because the impregnated phases coat the walls of the YSZ, the composites have a thermal expansion match close to that of the YSZ backbone [22]. The non-random structure also leads to good conductivity at relatively low metal loadings [27]. For random composites, there is essentially no conductivity below the 30-vol% percolation threshold [28]. Finally, composites formed by infiltration allow much greater flexibility in preparing electrodes with more complex microstructures, including layered structures having one metal coating another [16,29,30].

Stabilization of Cu-Based Anodes

Cu does not catalyze the formation of carbon fibers in the way that Ni does, making it possible to utilize hydrocarbons directly on Cu-based anodes without adding steam. Cu-ceria-YSZ composite anodes were found to exhibit stable performance in a wide variety of hydrocarbon fuels at 973 K, including ones that are liquids at room temperature [31]. Although Cu catalysts are active for the water-gas-shift and methanol-reforming reactions, the primary role of Cu in the anode composites appears to be that of an electronic conductor. Indeed, it is necessary to add a catalytic phase, such as ceria or mixed oxides of ceria [32], to the Cu-YSZ cermet in order to achieve reasonable power densities.

A major limitation of Cu-based anodes is that they tend to be unstable at high temperatures. Compared to Ni, Cu has a relatively low melting temperature and a low surface energy, resulting in rapid sintering of the Cu and loss of electrode conductivity at temperatures above 1073 K [15,16]. This sintering is shown in the Scanning Electron Micrographs of Fig. 2. Following reduction at 973 K, the Cu within the porous YSZ forms a well-connected network for electronic conduction. After briefly heating to 1173 K, the Cu phase has sintered into

unconnected particles. The resulting loss in conductivity leads to large increases in the ohmic resistances in the fuel-cell impedance spectra and a significant decrease in fuel-cell performance.

Since the ideal metal-based electrode would exhibit the carbon tolerance of Cu with the thermal stability of a more refractory metal, mixed-metal electrodes were investigated. Bimetallic electrodes can be made from metals that form alloys, like Cu and Ni [11,25,29] which are completely soluble, or from metals that remain as separate phases, such as Cu with either Cr [30] or Co [16]. Both types of electrodes were examined in our laboratory. The most promising of the mixed-metal electrodes that we examined were those composed of Cu and Co [16,33]. In many ways, Co has similar properties to that of Ni: Co has a slightly higher melting temperature than Ni, remains reduced under similar conditions as that of Ni, and forms carbon fibers in the presence of dry methane. Unlike Ni, Co has limited solubility with Cu at SOFC operating temperatures. Finally, free-energy considerations indicate that Cu will segregate to the surface of Co [34].

Anodes based on Cu-Co mixtures can be prepared by co-impregnation of porous YSZ with Cu and Co salts, followed by reduction of salts to the metals [33]; but the metal phase of composites formed in this manner will likely be random mixtures of Cu and Co crystallites. If the Cu phase sinters, the entire composite is likely to lose conductivity unless the Co phase itself forms a conductive network in the electrode. To ensure that a conductive network is established within the Co phase, we added the metals separately, using electrodeposition to add the second metal as a coating on the first. The initial intent was to prepare Co cermets, then electroplate the Co with Cu. However, Cu plating into a porous substrate is much more difficult than Co plating. Furthermore, X-ray Photoelectron Spectra (XPS) of a 250-nm Co film on a Cu plate showed that Cu migrates through the Co film above 873 K to form a Cu overlayer. Therefore, we were able to

achieve a layered structure like that shown in Fig. 3 by plating Co onto the Cu cermet and then heating the structure to 873 K in H_2 [16].

Fig. 4 shows a plot of the ohmic resistances of two fuel cells, one with only Cu in the anode and the other plated with Co, as a function of time at 1173 K. Both cells contained 18-vol% metal, with the Co-plated electrode having 13-vol% Cu and 5-vol% Co. The cells in this study used an electrolyte thickness of 300 μ m, which, together with the leads, contributed 0.5 $\Omega \cdot cm^2$ to the ohmic resistance. While the ohmic resistance of the Cu-only cell increased rapidly with time due to sintering of the Cu phase, the Cu-Co cell exhibited no change in performance over a period of 40 h, even though this is a much higher temperature than that targeted for operation of these cells.

The Cu-Co system also exhibited high tolerance towards carbon fiber formation. A Co cermet formed large amounts of carbon when exposed to dry methane at 1073 K for 3 h, but the Co-plated Cu electrode showed no observable carbon formation under the same conditions, as shown in the photographs in Fig. 5. While it is unclear whether the Cu-Co electrode would continue to show stability against carbon formation for long periods of time, a 50:50 Cu-Co electrode formed by co-impregnation was shown to exhibit stable performance in humidified CH_4 (3% H_2O) for at least 500 h at 1073 K and low fuel utilization [33]. This suggests that the free energy associated with Cu overlayers on the Co is sufficient to form a very effective barrier that prevents carbon formation.

Ceramic Anodes

Because oxides cannot dissolve carbon and therefore cannot form carbon fibers, anodes based on conductive ceramics offer another approach to direct-utilization fuel cells. Many oxides have high melting temperatures, so that the thermal stability problem associated with Cu could

be solved by the appropriate choice of oxides. An additional advantage to using ceramic anodes is that they should be redox stable, avoiding the potentially catastrophic problems associated with oxidation of metal electrodes during start-up and shut-down cycles. Finally, the most commonly used SOFC cathode material is an oxide, Sr-doped $LaMnO_3$ (LSM), demonstrating that oxides can in principle be good electrodes.

While many oxide properties would appear to be ideal, good electrochemical performance has been difficult to achieve with ceramic anodes. First, it has been argued that a minimum electronic conductivity of 1 S/cm [17] is required in the electrode and few oxides are capable of providing this at anode $P(O_2)$, the oxygen pressure defined by equilibrium between H_2 and H_2O in the anode compartment. In addition to this problem, oxide conductivities are usually a strong function of $P(O_2)$. While the $P(O_2)$ remains essentially 0.2 atm at an SOFC cathode, the $P(O_2)$ can vary by many orders of magnitude at the anode, depending on the temperature and H_2:H_2O ratio. (At the anode, $P(O_2)$ can easily vary from 10^{-15} to 10^{-25} atm.) Another challenge with ceramic anodes is that few oxides exhibit reasonable catalytic activity for oxidation. Therefore, obtaining good electronic conductivity and good catalytic activity, in the same ceramic material, has proven to be difficult.

There has been an intense effort to identify perovskites suitable for anode materials [35-40]. Most of these studies have focused on double perovskites containing a mixture of cations at the B site, with the objective being to obtain complementary functionality from the cations. Despite this effort to develop new ceramic materials [17], the only oxide that has been reported to have both good conductivity and catalytic activity is the double perovskite, $Sr_2MgMoO_{6-\delta}$ [40]. However, because all of the testing with this material has been performed with current collectors of Pt, a highly active oxidation catalyst, it is still uncertain whether this material truly

is a good electrocatalyst. Certainly, it would be very exciting if $Sr_2MgMoO_{6-\delta}$ is found to be a highly active catalyst, since none of the individual oxides making up this material exhibit high catalytic activity for hydrocarbon oxidation.

Rather than looking for new materials with novel properties, we have been working to separate the problems of electronic conduction and catalytic activity by preparing anodes with two distinct layers: a thin functional layer optimized for catalytic activity near the electrolyte and a thicker conduction layer on top of the functional layer, as shown diagrammatically in Fig. 6 [41]. We chose to make the thickness of the functional layer to be approximately 10 μm, since the electrochemical reactions in a high-performance electrode occur primarily within this distance from the electrolyte. Using a reasonable target of 0.6 W/cm^2 for the maximum power density (0.6 W/cm^2 corresponds to a total cell impedance of approximately 0.5 $\Omega \cdot cm^2$), the ohmic losses in the functional layer must be less than 0.1 $\Omega \cdot cm^2$. For a layer 10-μm thick, this goal is met so long as the material has a conductivity greater than 0.01 S/cm, a value that is relatively easy to reach. Since the conduction layer is only required for carrying electrons away from the functional layer, we postulated that any porous material with sufficient conductivity could be used.

In our initial tests of the concept, we prepared the functional layer by impregnating 1 wt% Pd and 40 wt% ceria into a 65% porous YSZ [41]. Earlier measurements of ceria impregnated into porous YSZ at a loading of 15-vol% had indicated that this composite would have a conductivity of 0.019 S/cm at 973 K in flowing H_2 [15], demonstrating that ceria/YSZ should have sufficient conductivity for a thin functional layer, without requiring the addition of a metal. Pd was added in dopant quantities because Pd/ceria is one of the most active oxidation catalysts known, exhibiting the lowest light-off temperature for CH_4 among heterogeneous

catalysts. For the conduction layer, we used either Ag paste, a good conductor with poor activity for oxidation catalysis, or a porous layer of $La_{0.3}Sr_{0.7}TiO_3$ (LST), a ceramic material that does not undergo solid-state reactions with YSZ [42,43] and has good electronic conductivity under reducing conditions.

Fig. 7 shows V-i polarization curves and impedance spectra in humidified H_2 (3% H_2O) for a cell having the functional layer described above with Ag paste as the conduction layer. The cell had a 50-µm YSZ electrolyte and 300-µm cathode made by impregnating 40-wt% $Sr_{0.2}La_{0.8}FeO_3$ (LSF) into porous YSZ [23]. While the V-i curves in Fig. 7a) exhibit a dramatic drop in the voltage for current densities above 1.2 A/cm^2, probably due to diffusion limitations for H_2 in the Ag paste, the performance characteristics are otherwise very good. For example, the data indicate maximum power densities of 350 mW/cm^2 at 923 K and 520 mW/cm^2 at 973 K. In good agreement with the V-i curves, the open-circuit impedance data at 973 K indicate that the total Area Specific Resistance (ASR) of the cell was 0.57 $\Omega \cdot$cm^2. Since the resistance of the 50-µm electrolyte can be calculated to be 0.27 $\Omega \cdot$cm^2 at 973 K and the impedance of the LSF-YSZ cathode has been estimated to be 0.1 $\Omega \cdot$cm^2 at this temperature, the anode losses are only 0.2 $\Omega \cdot$cm^2. Obviously, an anode that uses Ag paste as the conduction layer is not entirely ceramic; but cell performance was not significantly affected by replacing the Ag with a porous layer of LST [41].

The presence of a catalytic metal is essential for obtaining high performance levels in the functional layer, as shown in Fig. 8. The figure compares results in humidified H_2 at 973 K for three essentially identical cells with 12-µm functional layers, except that one cell contained only 40-wt% ceria and the other two had either 1-wt% Pd or 1-wt% Ni in addition to the ceria. The maximum power density of the cell with the ceria-only anode was 110 mW/cm^2 and the

impedance data demonstrate that most of the cell losses are associated with electrode polarization. The cell performance improved dramatically upon the addition of Pd and Ni, to maximum power densities of 520 mW/cm^2 and 420 mW/cm^2, respectively. Essentially all of the improvement is associated with a decrease in the electrode impedances, from more than 1.2 $\Omega \cdot cm^2$ when no metal was added to 0.25 $\Omega \cdot cm^2$ upon the addition of Pd and 0.35 $\Omega \cdot cm^2$ upon the addition of Ni. While there was a slight decrease in the ohmic resistance upon the addition of the catalytic metals, the primary change that occurred upon the addition of Pd or Ni was the loss of a large arc at 0.2 Hz in the Cole-Cole plots.

The presence of a catalyst is especially important when operating the cells in dry CH_4 at 973 K. Fig. 9 shows V-i polarization curves for 12-μm anodes with 40 wt% ceria, with and without 1% Pd. The Pd-containing cell achieved a maximum power density of 335 mW/cm^2, while the maximum power density in the ceria-only cell was 9 mW/cm^2. There are several remarkable features to the performance of the Pd-containing anode. In addition to the fact that its anode impedance in CH_4 approaches its impedance in H_2, the open-circuit voltage of this cell, 1.25 V, is higher than we could achieve operating on reformate. Furthermore, the Pd/ceria cell was stable in dry methane, even at open circuit where no steam is generated.

Future Directions

While the traditional Ni-YSZ composites exhibit excellent performance characteristics for SOFC operation in H_2 and syngas, there could be significant advantages to choosing alternative anode materials for achieving sulfur and carbon tolerance, as well as redox stability. In this review, we have tried to demonstrate that possibilities still remain for developing novel anode compositions and microstructures, especially for application with direct utilization of hydrocarbons.

In the first part of this paper, we have shown that it is possible to use layered structures within metal-based composites, with each layer playing a different role in achieving the desired electrode properties. Our studies focused on stabilizing Cu-based anodes, with the goal of achieving improved thermal stability, while retaining the chemical stability of Cu. There are obviously many other metal combinations that could be considered, beyond what we have examined. Furthermore, depending on the application, the targeted properties may be different from those discussed here.

The second part of this paper focused on separating the electrodes into two layers, a functional layer for optimal electrocatalysis and a thicker conduction layer for current collection. While the concept of a functional layer is certainly not new [44], it is not typical to use a completely different set of materials in each layer. By considering the required properties for each layer separately, it is possible to maximize the desired properties of the electrode. We would again like to emphasize that the results reported here were simply a demonstration of the concepts. Significant improvements are certainly possible, especially if the porous YSZ in the functional layer can be replaced with a mixed conducting material, so as to allow more flexibility in choosing oxidation catalysts.

Acknowledgements

This work was funded by the U.S. Department of Energy's Hydrogen Fuel Initiative (Grant DE-FG02-05ER15721).

References

1) EG&G Technical Services, Inc. *Fuel Cell Handbook 7th Edition*, DOE-NETL, U.S. Department of Energy, Office of Fossil Energy, National Energy Technology Laboratory, Morgantown, WV, 2004, sec. 1, pp. 12-14.

2) J. Larminie and A. Dicks, *Fuel Cell Systems Explained*, 2nd edn., 2003, ch. 3, pp. 51-52.

3) N. Q. Minh, *Solid State Ionics*, 2004, **174**, 271.

4) J. R. Rostrup-Nielsen, J. B. Hansen, S. Helveg, N. Christiansen, and A.-K. Jannasch, *Appl. Phys. A*, 2006, **85**, 427.

5) S. McIntosh, J. M. Vohs, and R. J. Gorte, *J. Electrochem. Soc.*, 2003, **150**, A1305.

6) S. Park, J. M. Vohs, and R. J. Gorte, *Nature*, 2000, **404**, 265.

7) S. McIntosh and R. J. Gorte, *Chem. Rev.*, 2004, **104**, 4845.

8) T. Kim, G. Liu, M. Boaro, S.-I. Lee, J. M. Vohs, R. J. Gorte, O. H. Al-Madhi, and B. O. Dabbousi, *J. Power Sources*, 2006, **155**, 231.

9) M. L. Toebes, J. H. Bitter, A. J. van Dillen, and K. P. de Jong, *Catal. Today*, 2002, **76**, 33.

10) C. H. Toh, P. R. Munroe, D. J. Young, and K. Foger, *Mater. High Temp.*, 2003, **20**, 129.

11) H. Kim, C. Lu, W. L. Worrell, J. M. Vohs, and R. J. Gorte, *J. Electrochem. Soc.*, 2002, **149**, A247.

12) EG&G Technical Services, Inc. *Fuel Cell Handbook 7th Edition*, DOE-NETL, U.S. Department of Energy, Office of Fossil Energy, National Energy Technology Laboratory, Morgantown, WV, 2004, sec. 8, p. 24.

13) R. J. Farrauto and C.H. Bartholomew, *Fundamentals of Industrial Catalytic Processes*, Blackie Academic and Professional, London, 1st ed., 1997, pp. 341-357.

14) R. T. K. Baker and J. J. Chuldzinski, Jr., *J. Phys. Chem.*, 1986, **90**, 4734.

15) S. Jung, C. Lu, H. He, K. Ahn, R.J. Gorte, and J.M. Vohs, *J. Power Sources*, 2006, **154**, 42.

16) M. D. Gross, J. M. Vohs, and R. J. Gorte, *Electrochimica Acta*, 2007, **52**, 1951.

17) A. Atkinson, S Barnett, R. J. Gorte, J.T.S. Irvine, A.J. McEvoy, M.B. Mogensen, S. Singhal, and J. Vohs, *Nature Materials*, 2004, **3**, 17.

18) Minh, N.Q. *J. Am. Ceram. Soc.*, 1993, **76**, 563.

19) R. Craciun, R.J. Gorte, J.M. Vohs, C. Wang, and W.L. Worrell, *J. Electrochem. Soc.*, 1999, **146**, 4019.

20) R. J. Gorte, S. Park, J. M. Vohs, and C. Wang, *Advanced Materials*, 2000, **12**, 1465.

21) S. Park, R. J. Gorte, and J. M. Vohs, *J. Electrochem. Soc.*, 2001, **148**, A443.

22) Y. Huang, K. Ahn, J. M. Vohs, and R. J. Gorte, *J. Electrochem. Soc.*, 2004, **151**, A1592.

23) Y. Huang, J. M. Vohs, and R. J. Gorte, *J. Electrochem. Soc.*, 2004, **151**, A646.

24) Y. Huang, J. M. Vohs, and R. J. Gorte, *J. Electrochem. Soc.*, 2006, **153**, A951.

25) S.-I. Lee, J. M. Vohs, and R. J. Gorte, *J. Electrochem. Soc.*, 2004, **151**, A1319.

26) S. McIntosh, J. M. Vohs, and R. J. Gorte, *Electrochimica Acta*, 2002, **47**, 3815.

27) H. He, Y. Huang, J. Regal, M. Boaro, J. M. Vohs, and R. J. Gorte, J. Am. Cer. Soc., 2004, **87**, 331.

28) D.W. Dees, T.D. Claar, T.E. Easler, D.C. Fee, F. C. Mrazek, *J. Electrochem. Soc.*, 1987, **134**, 2141.

29) S. Jung, M. D. Gross, R. J. Gorte, and J. M. Vohs, *J. Electrochem. Soc.*, 2006, **153**, A1539.

30) M. D. Gross, J. M. Vohs, and R. J. Gorte, *J. Electrochem. Soc.*, 2006, **153**, A1386.

31) H. Kim, S. Park, J. M. Vohs, and R. J. Gorte, *J. Electrochem. Soc.*, 2001, **148**, A693.

32) K. Ahn, H. He, J. M. Vohs, and R. J. Gorte, *Electrochem. Solid-State Lett.*, 2005, **8**, A414.

33) S.-I. Lee, K. Ahn, J. M. Vohs, and R. J. Gorte, *Electrochem. Solid-State Lett.*, 2005, **8**, A48.

34) S. -K. Kim, J. -S. Kim, J. Y. Han, J. M. Seo, C. K. Lee, and S. C. Hong, *Surf. Sci.*, 2000, **453**, 47.

35) S. Tao, and J. T. S. Irvine, *Chem. Rec.*, 2004, **4**, 83.

36) J. Liu, B. D. Madsen, A. Ji, and S. A. Barnett, *Electrochem. Solid-State Lett.*, 2002, **5**, A122.

37) O. A. Marina, N. L. Canfield, and J. W. Stevenson, *Solid State Ionics*, 2002, **149**, 21.

38) J. Sfeir, P. A. Buffat, P. Mockli, N. Xanthopoulos, R. Vasquez, H. J. Mathieu, J. Van herle, and K. R. Thampi, *J. Catal.*, 2001, **202**, 229.

39) Y. H. Huang, R. I. Dass, J. C. Denyszyn, and J. B. Goodenough, *J. Electrochem. Soc.*, 2006, **153**, A1266..

40) R. Mukundan, E. L. Brosha, and F. H. Garzon, *Electrochem. Solid-State Lett.*, 2004, **7**, A5.

41) M. D. Gross, J. M. Vohs, and R. J. Gorte, *Electrochem. Solid-State Lett.*, 2007, **10**, B65.

42) H. He, Y. Huang, J. M. Vohs, and R. J. Gorte, *Solid State Ionics*, 2004, **175**, 171.

43) Kipyung Ahn, Sukwon Jung, John M. Vohs, Raymond J. Gorte, *Ceram. Int.*, in press.

44) F. Zhao and A. V. Virkar, *J. Power Sources*, 2004, **141**, 79.

Figure captions

Fig. 1 Schematic of composite fabrication by impregnation.

Fig. 2 Scanning Electron Micrographs of a Cu-CeO_2-YSZ composite (18 vol% Cu, 9 vol% ceria) following reduction in humidified H_2 (3% H_2O) at (a) 973 K for 2h and (b) 1173 K for 5h.

Fig. 3 Schematic of Cu-Co-Cu layered structure fabrication by electrodeposition.

Fig. 4 Ohmic resistance measurements at 1173 K in humidified (3% H_2O) H_2 as a function of time for (♦) Cu-CeO_2-YSZ (18 vol% Cu) and (●) Co-Cu-CeO_2-YSZ (5 vol% electrodeposited Co and 13 vol% Cu). The electrolyte was 300 μm thick YSZ.

Fig. 5 Photographs of (a) Cu-Co-CeO_2-YSZ (5 vol% electrodeposited Co, 13 vol% Cu) and (b) Co-CeO_2-YSZ (18 vol% Co) after reduction in dry H_2 at 1073 K and exposure to dry CH_4 for 3 h at 1073 K.

Fig. 6 Schematic of a proposal for ceramic anodes using a catalytically active functional layer.

Fig. 7 (a) V-i polarization curves and (b) impedance spectra on a 12 μm thick CeO_2-Pd-YSZ anode (40 wt% CeO_2 and 1 wt% Pd) in humidified H_2 (3% H_2O), using Ag paste for current collection. Data are shown for the following temperatures: (○) 923 K, (◊) 973 K, (Δ) 1023 K, (□) 1073 K. The electrolyte was 50 μm thick YSZ and the cathode was impregnated LSF in 300 μm thick YSZ.

Fig. 8 (a) V-i polarization curves and (b) impedance spectra on 12 μm thick CeO_2-M-YSZ anodes with 40 wt% CeO_2 in humidified H_2 (3% H_2O). Data are shown for the following metal dopants (M): (○) no metal, (◊) 1 wt% Ni, and (Δ) 1 wt% Pd.

The electrolyte was 50 μm thick YSZ and the cathode was impregnated LSF in 300 μm thick YSZ. Ag paste was used for current collection.

Fig. 9 V-i polarization curves on 12 μm thick CeO_2-M-YSZ anodes with 40 wt% CeO_2 in dry CH_4. Data are shown for the following metal dopants: (○) no metal and (◊) 1 wt% Pd. The electrolyte was 50 μm thick YSZ and the cathode was impregnated LSF in 300 μm thick YSZ. Ag paste was used for current collection.

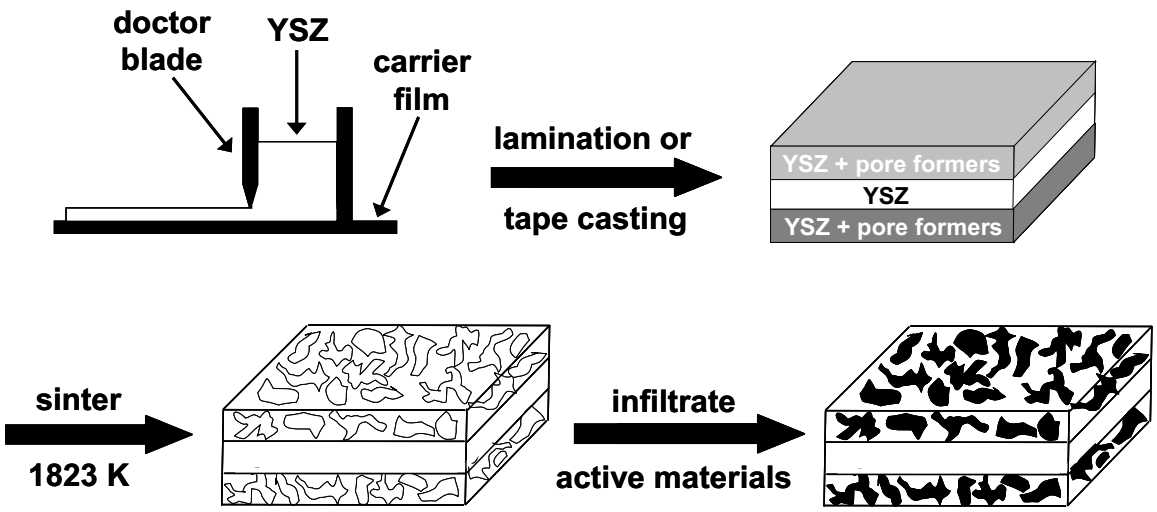
doctor blade
YSZ
carrier film
lamination or
tape casting
YSZ + pore formers
YSZ
YSZ + pore formers
sinter
1823 K
infiltrate
active materials

Fig. 1

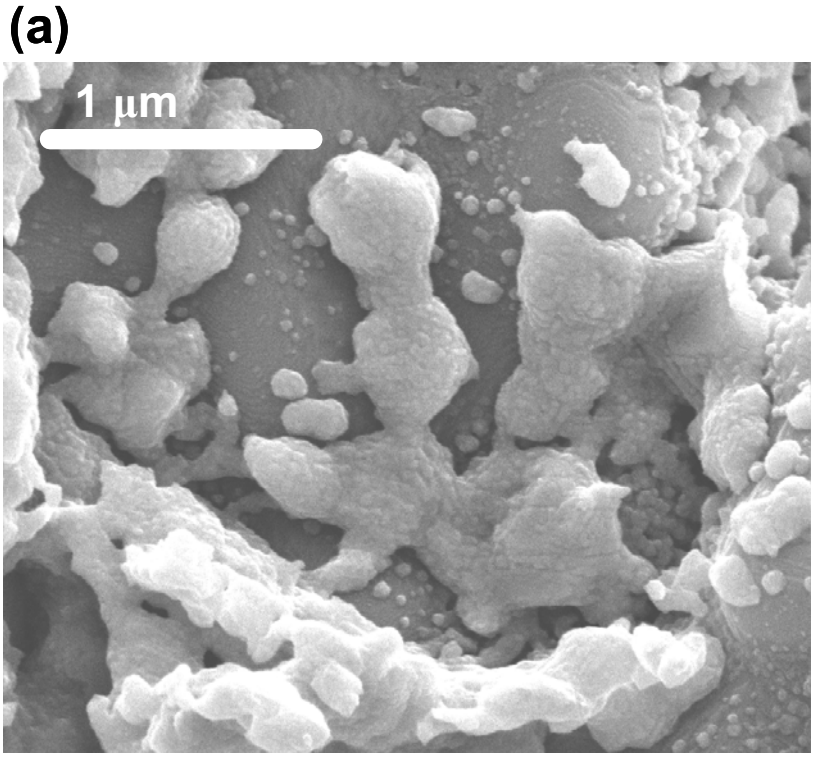
(a)
1 μm

Fig. 2a

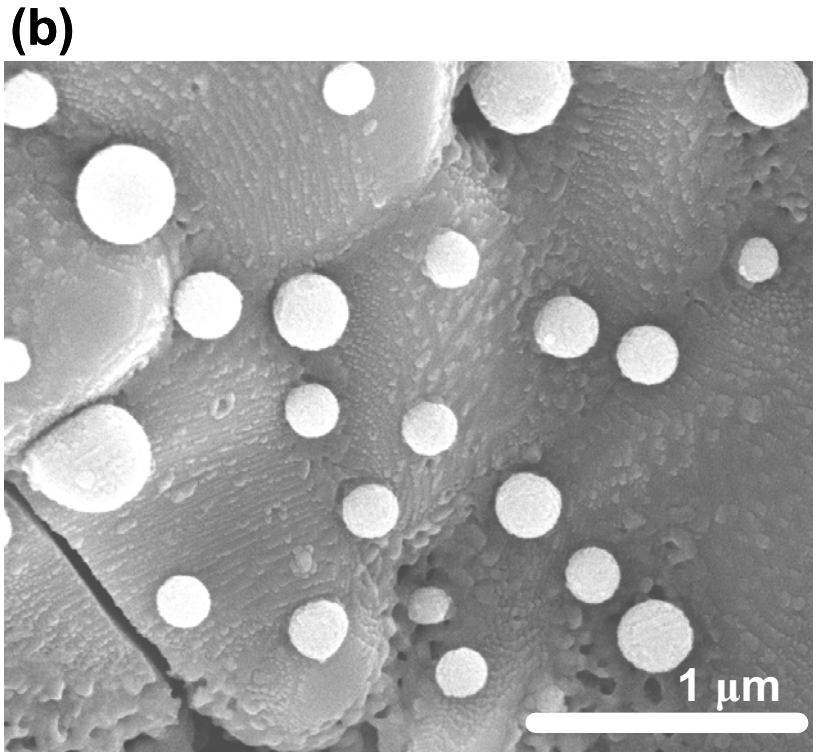
(b)
1 µm

Fig. 2b

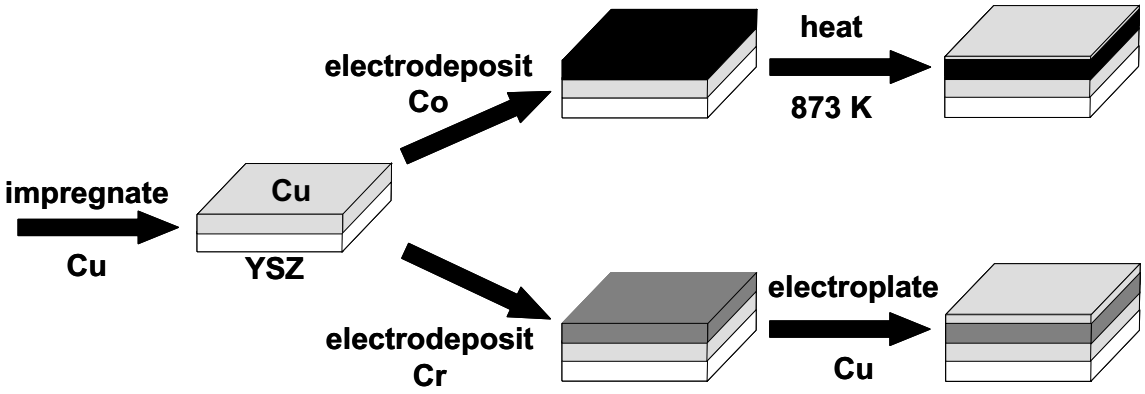
impregnate
Cu
Cu
YSZ
electrodeposit
Co
heat
873 K
electrodeposit
Cr
electroplate
Cu

Fig. 3

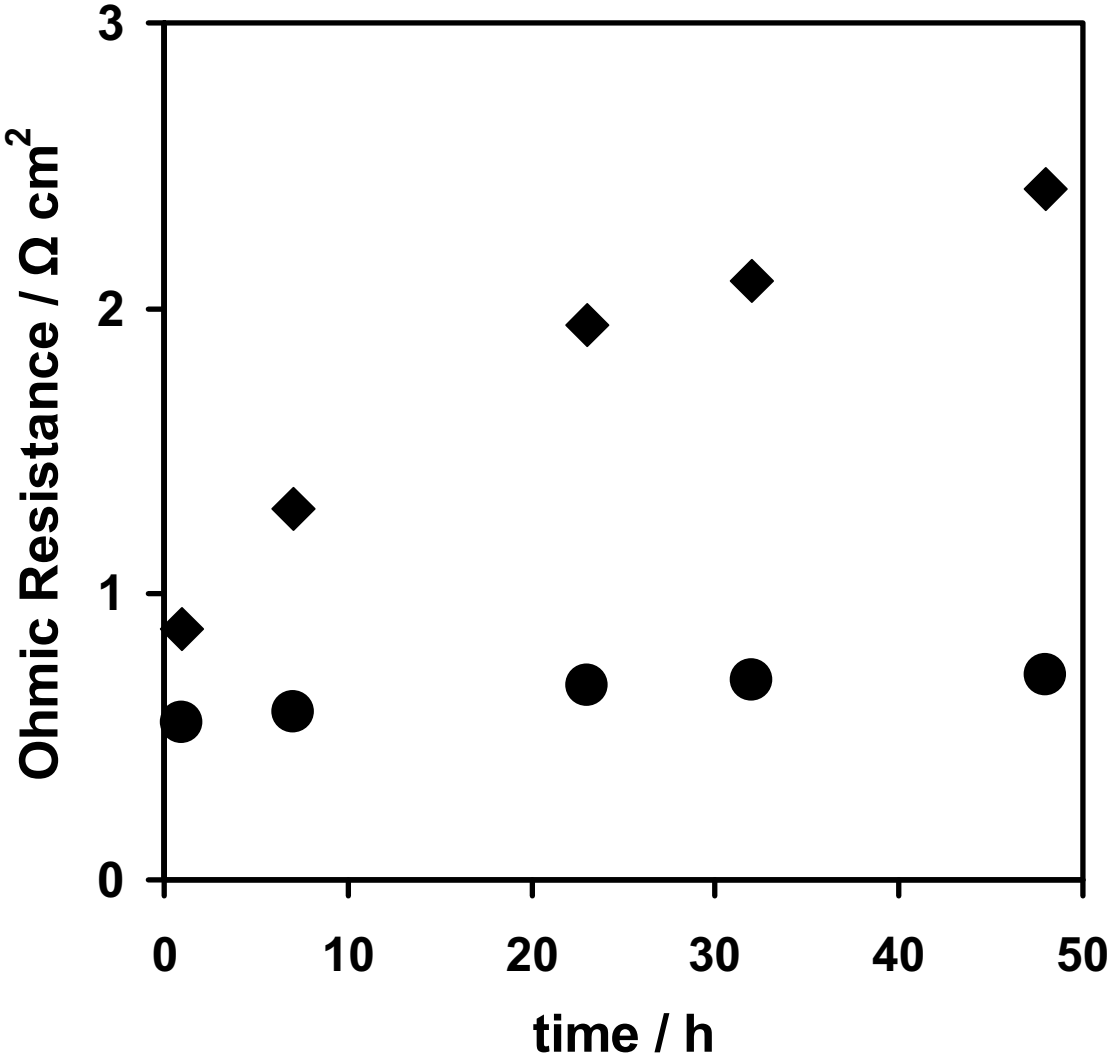

Fig. 4

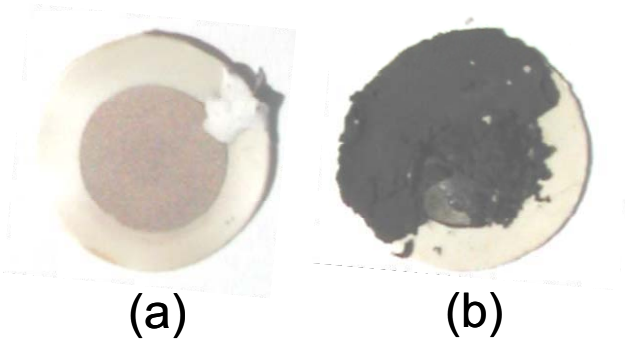
(a)
(b)

Fig. 5

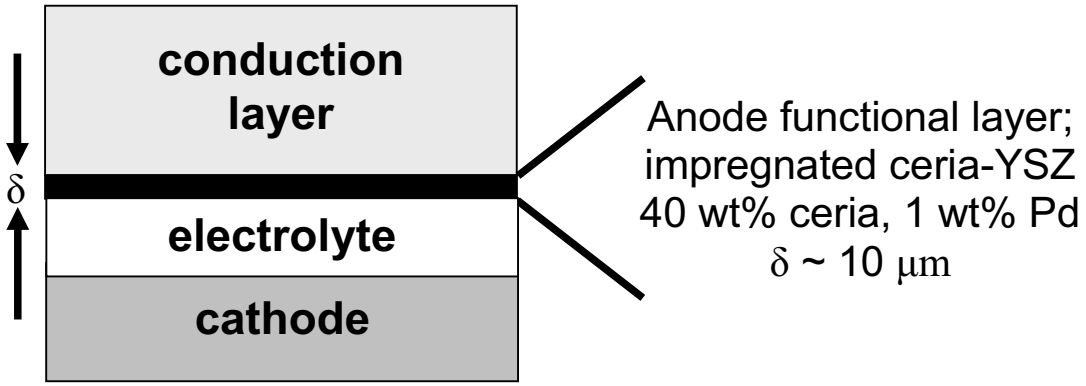
conduction layer
δ
electrolyte
cathode
Anode functional layer;
impregnated ceria-YSZ
40 wt% ceria, 1 wt% Pd
δ ~ 10 μm

Fig. 6

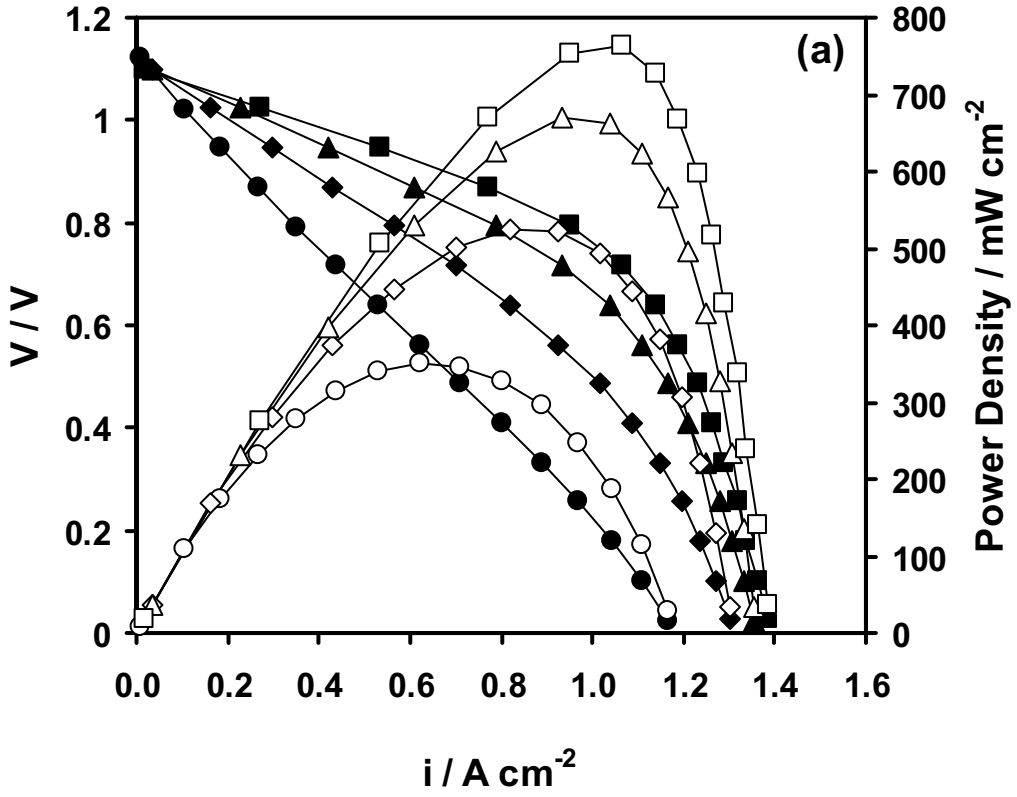
(a)
V / V
Power Density / mW cm-2
i / A cm-2
0
0.2
0.4
0.6
0.8
1
1.2
0
100
200
300
400
500
600
700
800
0.0
0.2
0.4
0.6
0.8
1.0
1.2
1.4
1.6

Fig. 7a

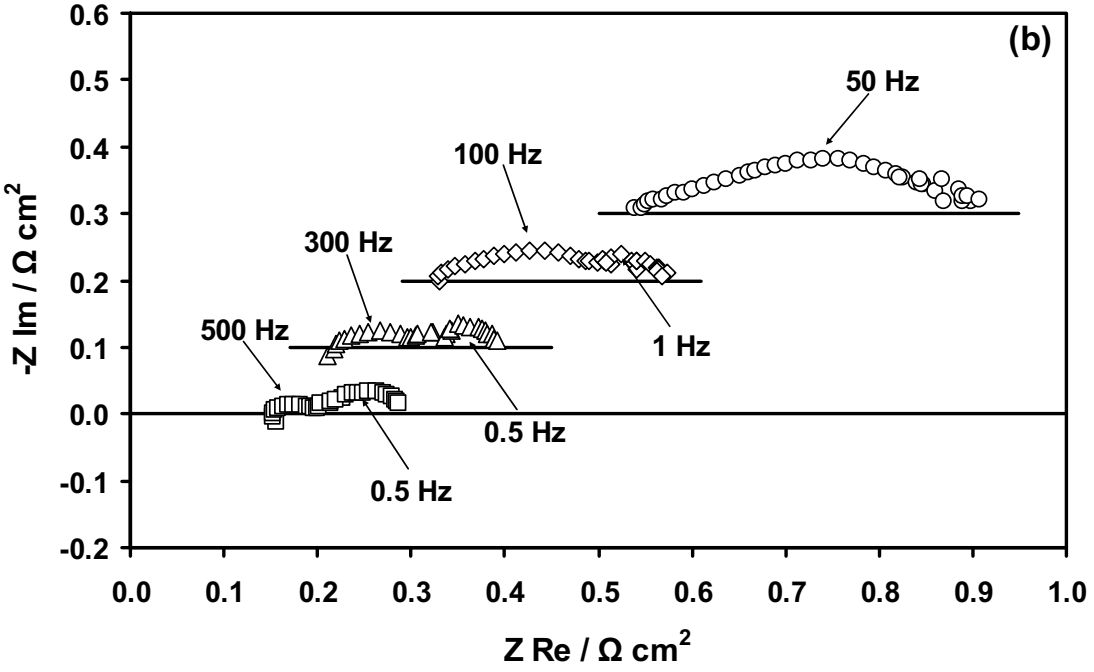
(b)
50 Hz
100 Hz
300 Hz
500 Hz
1 Hz
0.5 Hz
0.5 Hz
-Z Im / Ω cm2
Z Re / Ω cm2
0.6
0.5
0.4
0.3
0.2
0.1
0.0
-0.1
-0.2
0.0
0.1
0.2
0.3
0.4
0.5
0.6
0.7
0.8
0.9
1.0

Fig. 7b

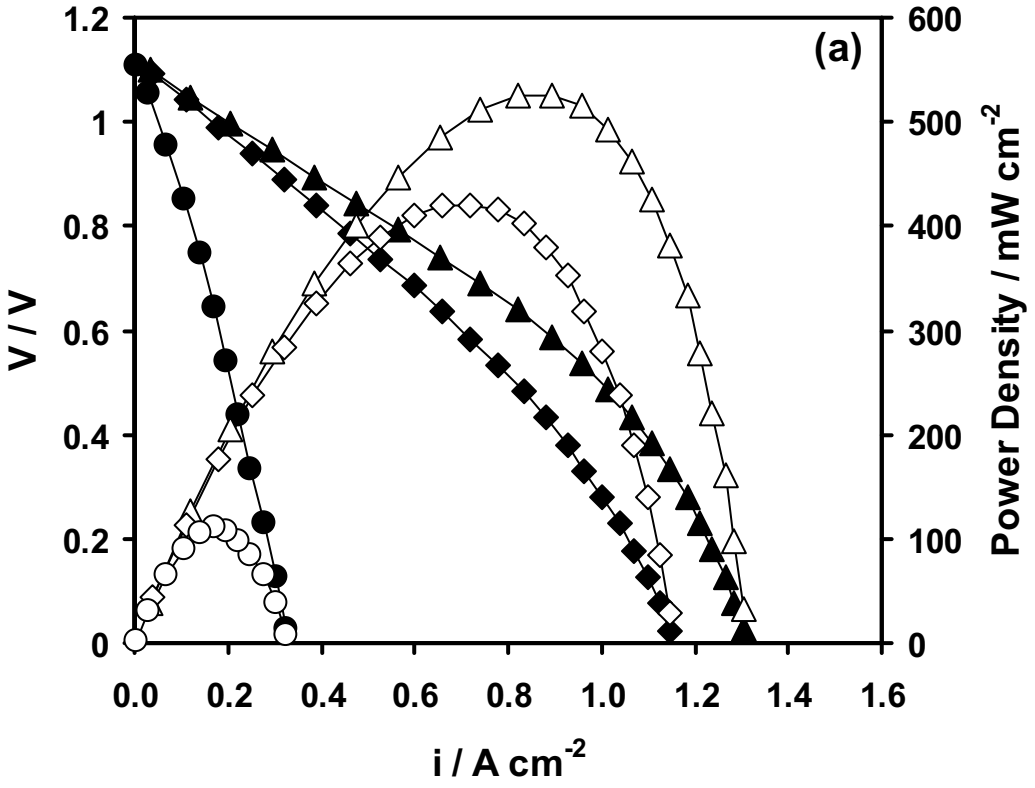
(a)
V / V
Power Density / mW cm-2
i / A cm-2
1.2
1
0.8
0.6
0.4
0.2
0
600
500
400
300
200
100
0
0.0
0.2
0.4
0.6
0.8
1.0
1.2
1.4
1.6

Fig. 8a

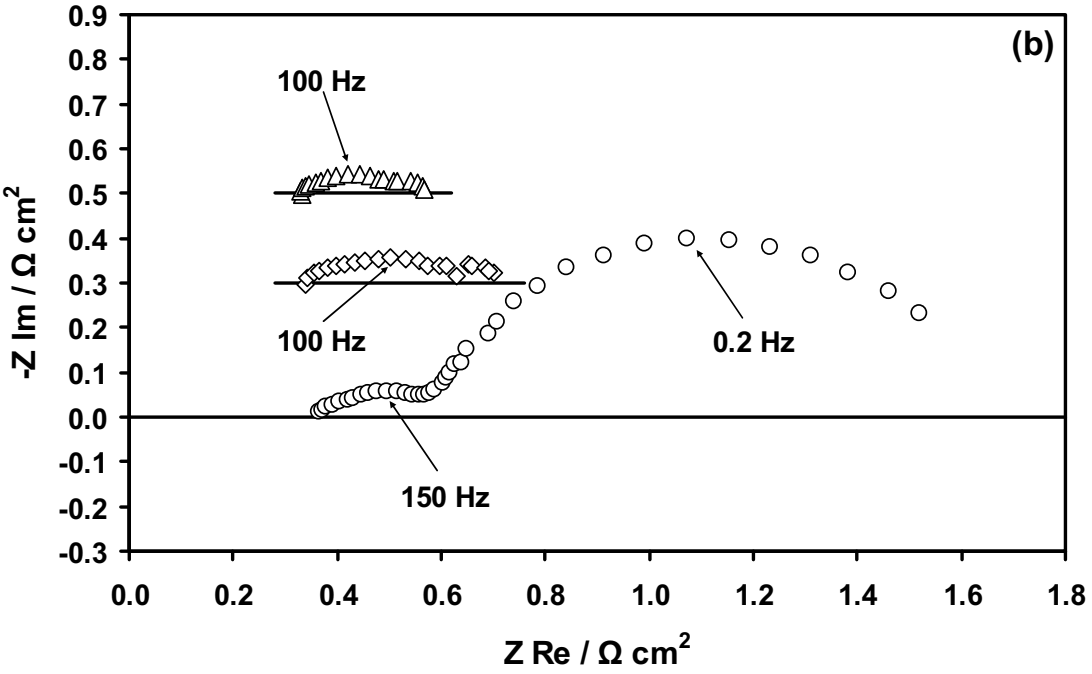
(b)
100 Hz
100 Hz
0.2 Hz
150 Hz
-Z Im / Ω cm2
Z Re / Ω cm2
0.9
0.8
0.7
0.6
0.5
0.4
0.3
0.2
0.1
0.0
-0.1
-0.2
-0.3
0.0
0.2
0.4
0.6
0.8
1.0
1.2
1.4
1.6
1.8

Fig. 8b

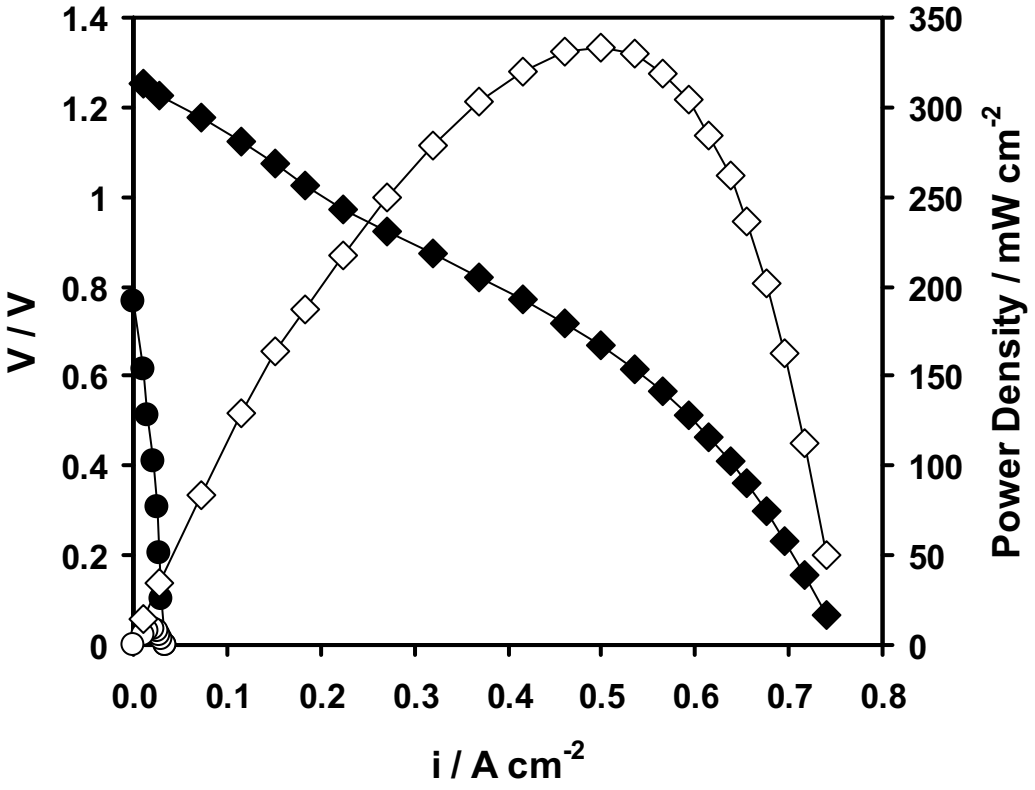
1.4
1.2
1
0.8
0.6
0.4
0.2
0
V / V
350
300
250
200
150
100
50
0
Power Density / mW cm-2
0.0
0.1
0.2
0.3
0.4
0.5
0.6
0.7
0.8
i / A cm-2

Fig. 9